

Experimental and analytical study on anchorage capacity between single-pole tower and RC foundation

S. Saito

Tokyo Electric Power Services Co., Ltd., Tokyo, Japan

T. Kamimoto & K. Yui

Tokyo Electric Power Company, Tokyo, Japan

ABSTRACT: Single-pole towers are used in engineering practice when there is not enough land to construct a conventional four-leg transmission tower. The load-bearing mechanism of the single-pole tower foundation system is quite different to the conventional type, which is subject to moment loads. Half-scale model experiments were conducted first using the same type of anchorage method between a single pole and reinforced concrete foundation. Two cases with different thickness of reinforced concrete cover were studied, and the results indicate the significance of the confinement effect on such anchorage systems. Finite element analyses were then conducted and successfully simulated the experimental results. Based on the understanding of failure mechanisms, which were studied both experimentally and via numerical analysis, a simplified design is proposed for the primary stage of the design.

1 INTRODUCTION

It is hard to obtain sufficient land to construct conventional four-leg transmission towers in cities. The single-pole type is used instead (Fig. 1). As both of these two types of tower foundations have steel-concrete composite structures, their capacities are dominated by the anchorage method between the steel superstructure and the reinforced concrete foundation.

Figure 2 illustrates the details of the anchorage method for single-pole towers. The single pole is fastened by means of a group of anchor bolts to a steel plate, which is embedded into the concrete body. Compared to conventional types of tower, the foundation of which is subjected to simple uplift and compressive loads, moment loads are applied directly to single-pole tower foundations. As a result, the failure mechanism for the latter one is much more complex when stressed by wind.

Yoshii et al. (1998) experimentally and analytically studied the failure mechanism of the conventional tower foundation, pointed out the significance of the occurrence and propagation of splitting cracks while the steel legs were pulled out, and developed a design formula defining the pull-out capacity. By contrast, a design method for single-pole towers is still required.

This paper strives to comprehend the failure mechanism of single-pole tower foundations so as to propose a design method to compute the maximum

moment that can be applied. As per the development of nonlinear mechanics of reinforced concrete, it is possible to analyze the performance of the tower foundation with finite element analysis. However, a simplified formula is still needed at the primary design stage. Thus, a scale model of the single-pole tower foundation will be tested so that the failure mechanism can be experimentally and analytically studied. Then a simplified design formula is proposed.

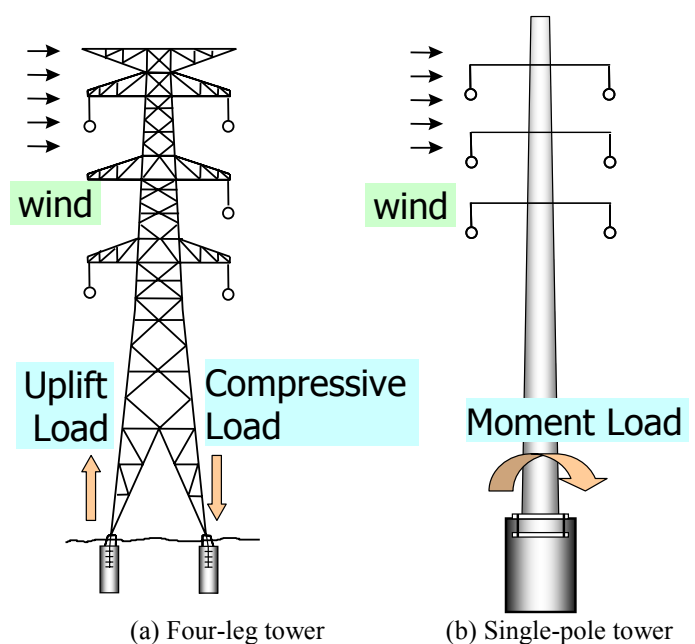


Figure 1. Transmission tower.

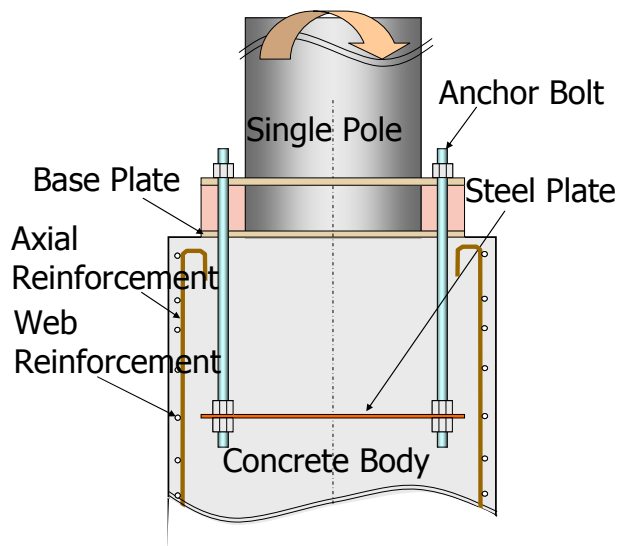


Figure 2. Anchorage between single pile and foundation.

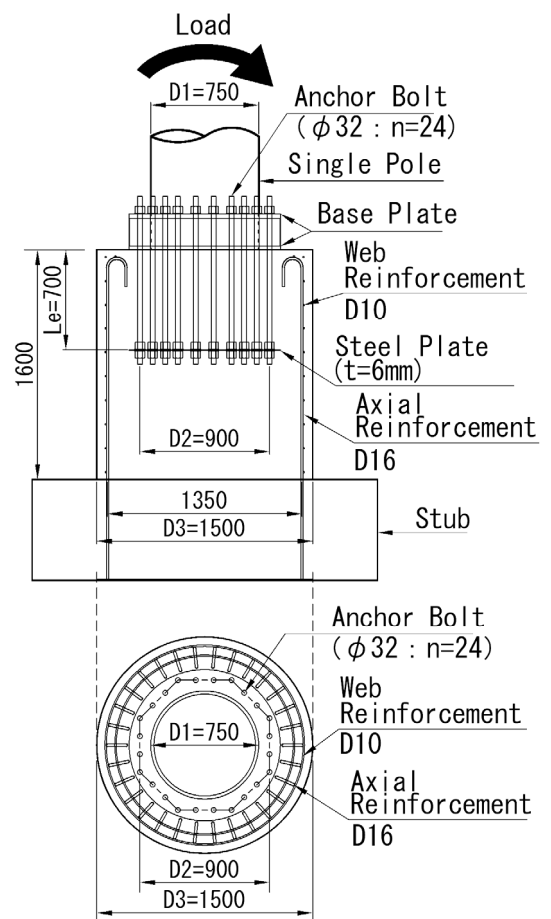
2 EXPERIMENTAL STUDY

2.1 Specimens and experiment setup

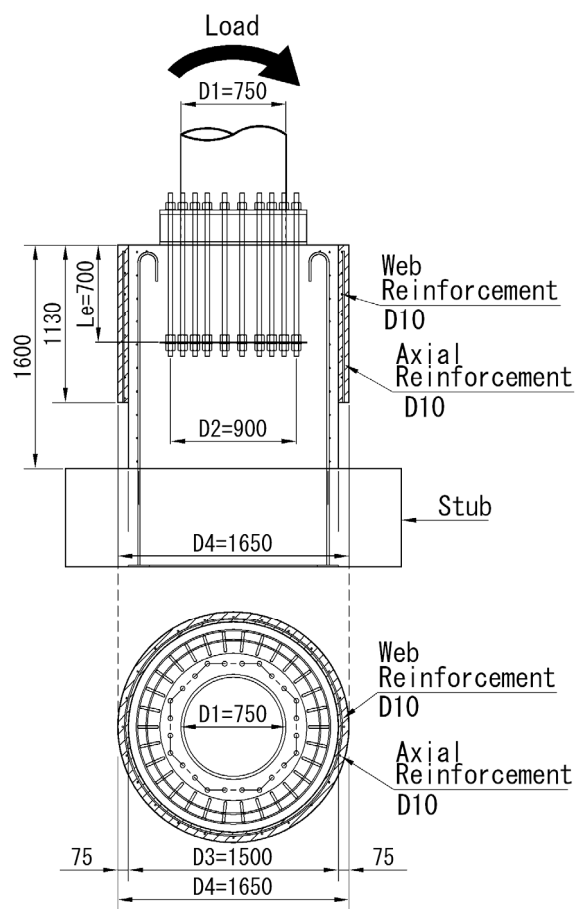
Half-scale model tests were conducted to study the anchorage capacity of a single-pole tower as per Figure 4. A 5-m high steel pipe was set up as the transmission tower, the pedestal of which was fastened with 24 steel bolts ($\phi 32$ -mm) around the circumference. All the other ends of these steel bolts were secured to a 6-mm thick steel plate. Figure 2 shows the details of the anchorage method.

The steel plate was embedded in a 1.6-m high reinforced concrete cylinder specimen, which was fixed in the ground with axial reinforcement. The embedded length of the anchor bolts was 0.7 m. Horizontal load was applied to the top of the steel pole to produce a moment on the anchorage system. The steel pole, anchor bolts and plates were designed to have appropriate capacity to cause anchorage failure before any yielding of these steel structure elements. Table 1 shows the size and material details for these steel elements.

Two reinforced concrete cylinder specimens were studied. M1-1 was set up as exactly half the size of a real tower, while a strengthened reinforced concrete part was used in M1-2 to study the strengthening effect as presented in Figure 3. Table 2 shows the size and material details for the two cases. The same sized steel elements as above were used in the two tests, both of which were anchored in the center of the concrete specimens. The weights of the steel poles were 2,630 kg for M1-1 and 4,070 kg for M1-2. It was expected that M1-2 would have a larger anchorage capacity than M1-1. Figure 3 shows the cross section and reinforcement arrangement. Table 3 shows the material details of the reinforcement used in the tests. Figure 5 shows the arrangement of displacement sensors and strain gauges.



(a) Specimen (M1-1)



(b) Specimen (M1-2)

Figure 3. Specimens.

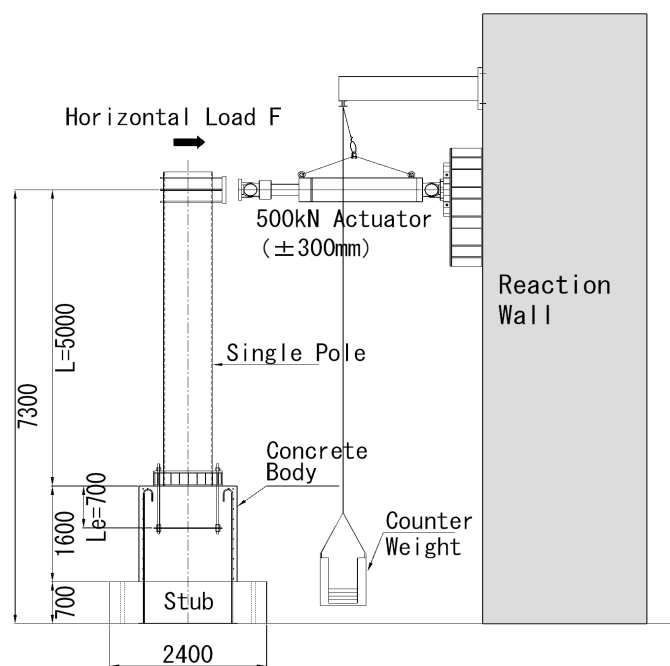


Figure 4. Experiment setup.

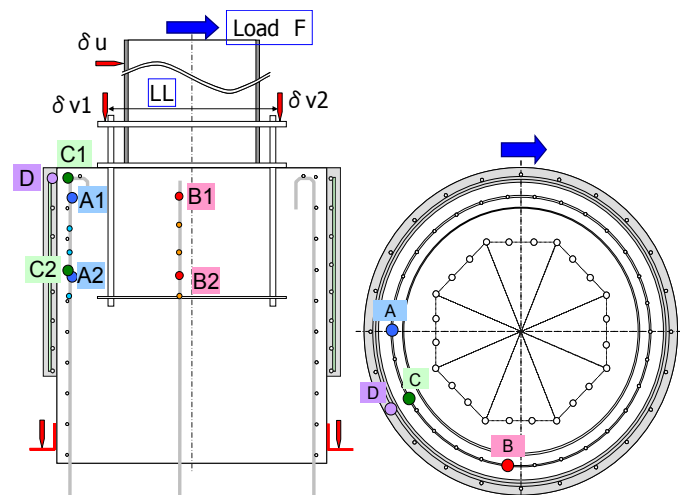


Figure 5. Positions of the measuring instruments.

Table 1. Size and material properties of steel elements used in the tests.

part	Diameter / thickness (mm)	Yield strength f_y (N/mm ²)	
		M1-1	M1-2
Single pole	22	330	330
Anchor bolt	32	1,039	1,039
Steel plate	6	534	734

Table 2. Size and material properties of concrete used in the tests.

No.	Diameter (mm)		Concrete f'_c (N/mm ²) Compressive strength	
	D3	D4	Original part	Strengthened part
M1-1	1500	-----	21.7	-----
M1-2	1500	1650	24.7	28.0

Table 3. Size and material properties of reinforcement used in the tests.

Di- ameter (mm)	TYPE	Yield strength f_y (N/mm ²)		Remarks
		M1-1	M1-2	
16	USD785	786	780	Axial reinforcement
10	SD295	345	358	Web reinforcement
				Web&Axial
10	SD345	-----	386	reinforcement in strengthened part

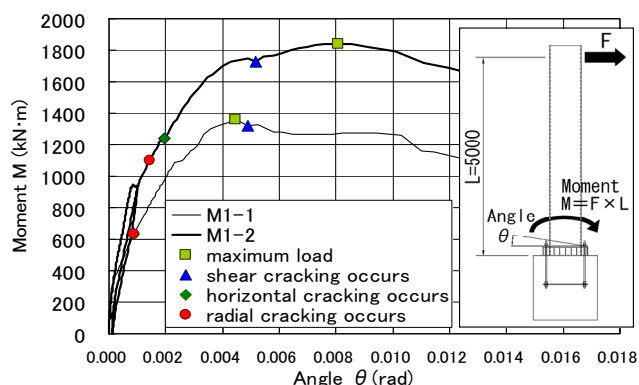


Figure 6. Moment load and rotational angle relationship.

2.2 Test results

The relationship between the moment load and angle of rotation of each specimen is shown in Figure 6. Here the moment load is defined as:

$$M = F \cdot L \quad (1)$$

where F is the horizontal load applied in the tests, and L is the height of the steel pole.

Furthermore, the angle of rotation is defined as:

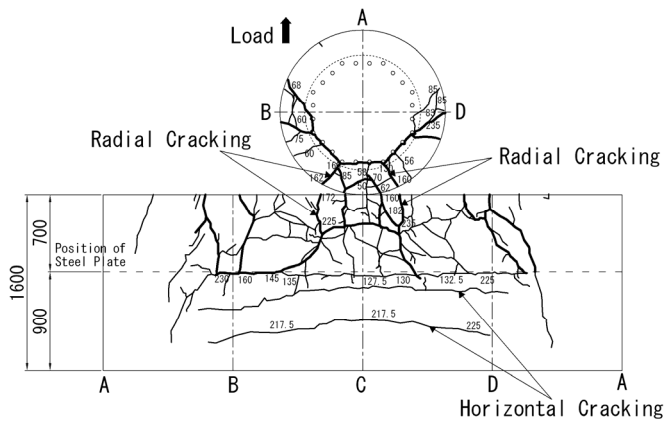
$$\theta = \frac{\delta_{v1} + \delta_{v2}}{LL} \quad (2)$$

where δ_{v1} and δ_{v2} denote the vertical displacement of the base plate, and LL is the displacement sensor length.

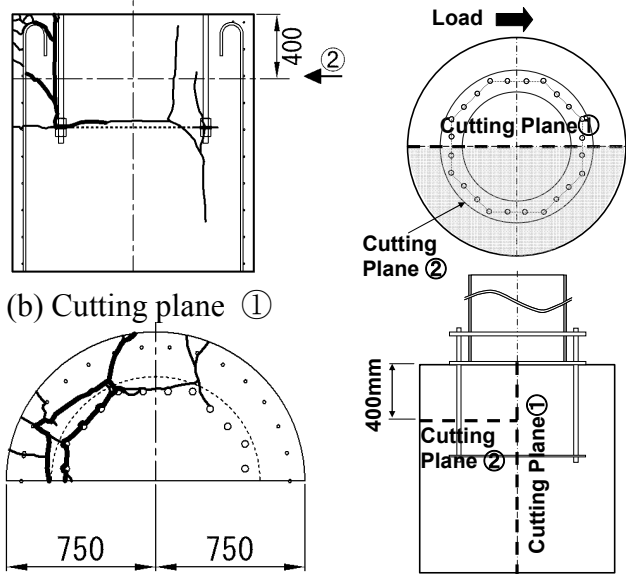
It was confirmed that M1-2 had a larger capacity than M1-1 as expected. The ultimate moments for specimens M1-1 and M1-2 were 1,357 kN·m and 1,840 kN·m respectively.

Figures 7 and 8 show the cracking pattern of each specimen at failure. In both cases, splitting cracks were found in the cylinder foundation along the radial directions starting from the anchorage bolt, coupled with a horizontal crack starting from the site of the embedded steel plate and a diagonal crack starting from the lug of the anchored bolt.

It was observed in the experiment that after the splitting crack penetrated the concrete cover, the specimen demonstrated shear failure of the foundation. Figure 9 shows the strain distribution of axial reinforcement of each specimen at peak loads. The



(a) Surface



(b) Cutting plane ①

(c) Cutting plane ②

Figure 7. Cracking of specimen M1-1.

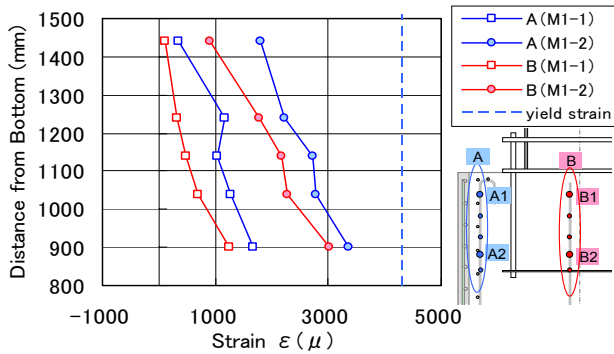
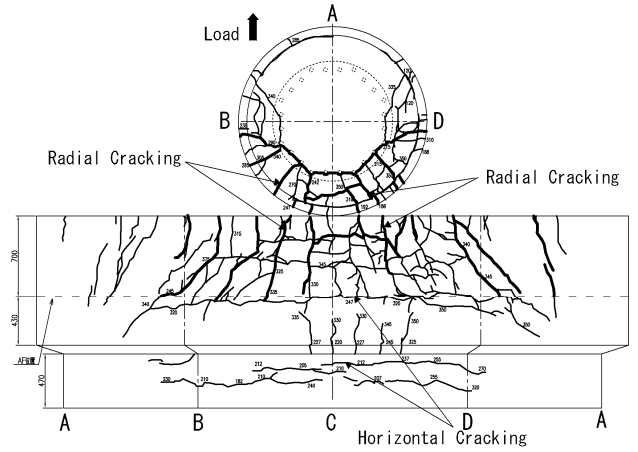


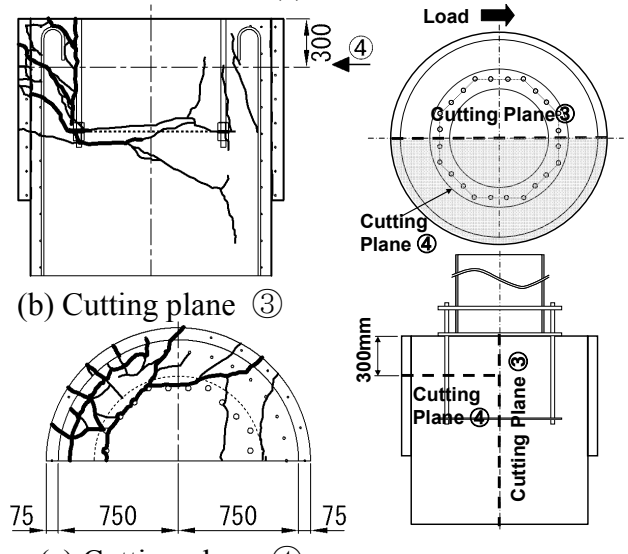
Figure 9. Strain distribution of axial reinforcement.

strain of axial reinforcement at the peak moment was far from the yield point (4,300 μ).

Figures 10 and 11 show the relationship between the loading moment and web reinforcement strain in these two cases. It is found that both specimens failed immediately after the web reinforcement yielded. Furthermore, the web reinforcement yielded at a much higher load in M1-2 than M1-1. This is because much more energy was needed for M1-2 to have the same splitting crack width at the same position, as it had a larger diameter of concrete cover of



(a) Surface



(b) Cutting plane ③

(c) Cutting plane ④

Figure 8. Cracking of specimen M1-2.

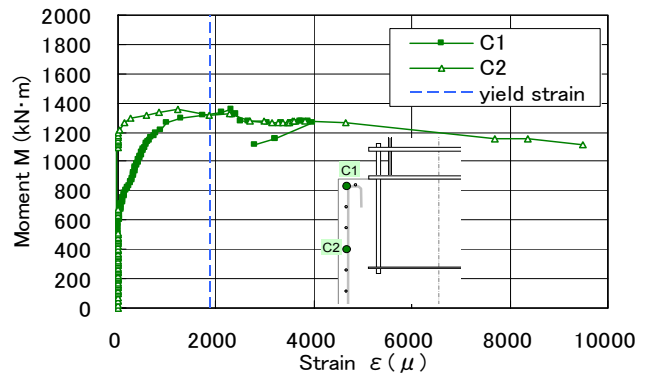


Figure 10. Strain on web reinforcement for M1-1.

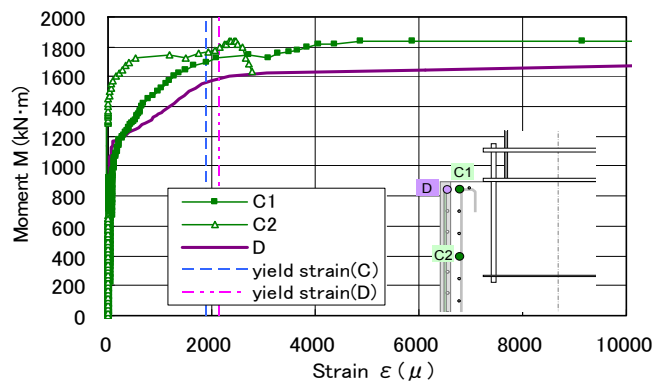


Figure 11. Strain on web reinforcement for M1-2.

steel bolts. Thus, the confinement level governs the ultimate state of anchorage performance.

3 ANALYTICAL STUDY

3.1 Computational tool

A 3D FEM code COM3 was used here to simulate the above model test, which was developed in the concrete laboratory at the University of Tokyo (Okamura & Maekawa 1991, Maekawa et al. 2003), while the graphics-based preprocess and post-process software for this code were developed at Tsinghua University. This software is convenient for establishing a mesh for reinforced concrete structures and steel-concrete composite structures, picking up the stress-strain data of each element, and displaying the damage and cracked state of the concrete (You et al. 2004).

The nonlinear reinforced concrete (RC) path-dependent constitutive equations have been integrated in the COM3 computation code. The 3D multi-directional fixed smeared cracking approach has been developed to treat the interaction between non-orthogonal cracks in concrete, such as the splitting cracks and shear cracks generated from the steel bolts in these cases. The spatial average constitutive models are installed to describe the mean response of reinforced concrete between cracks under tension, compression and shear force in the RC zone. The RC zoning procedure is applied here to take into account the crack dispersion caused by bonds between reinforcement and concrete. All the concrete models have been well verified in past research; thus, the authors skip the details, which are lined in the reference (Maekawa et al. 2003).

3.2 Simulation of the model test

Figures 12 and 13 show the finite element mesh for simulating the model test. A half side of the model with symmetric boundary conditions was established for analysis. The steel structural elements were simulated as elasto-plastic material; 3D-quadrilateral solid elements were used for the steel plate embedded in concrete, the single pole, and its pedestal, while 1D truss elements were used for the steel bolts. The diameters of the axial and web reinforcements were implicitly taken into account in the 3D solid concrete elements. Joint elements were used between the steel pedestal and concrete specimen in the analysis in order to ignore the cohesion between the two parts. The boundary conditions were set as per Figures 12 and 13.

Figure 14 shows the computed relationship between the applied moment and angle of rotation compared with the experiment data. It was found

that the experimental capacity was accurately simulated in the analysis. The computed peak moments for specimens M1-1 and M1-2 are 1,378 kN•m and 1,962 kN•m. As the deformation or principle strain situations for both analyses were similar, the figure of specimen M1-1 is shown as one example.

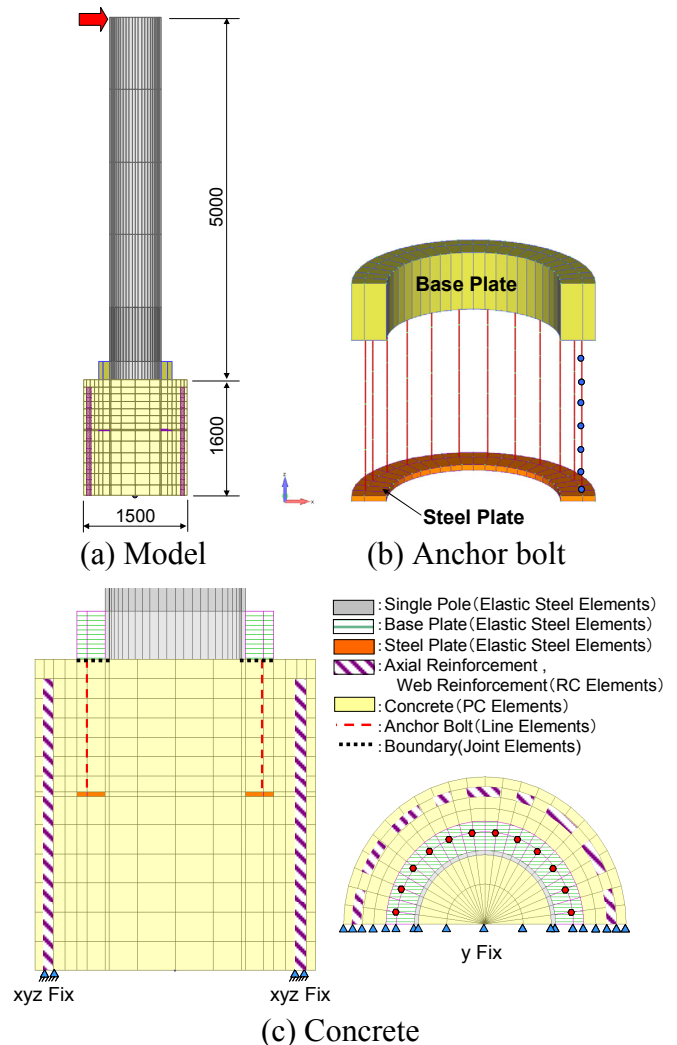


Figure 12. FEM modeling (M1-1).

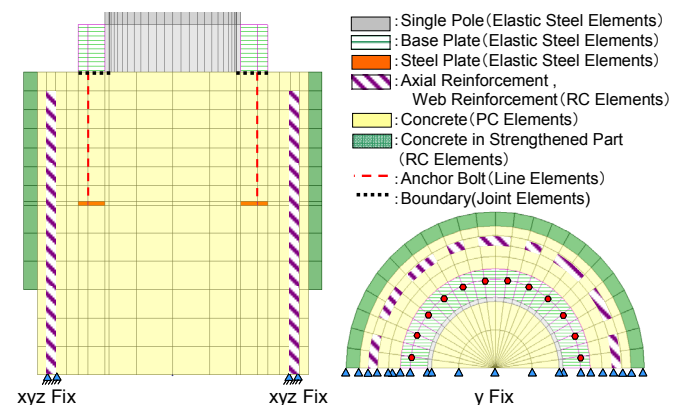


Figure 13. FEM modeling (M1-2).

The analytical deformation (Fig. 16) clearly denoted that when moment was applied in such an anchorage system, the anchoring part, including the embedded plate and steel bolts, tended to be pulled out of the concrete cylinder. Thus, large deformation

and cracks were produced in the tension side of the concrete specimen.

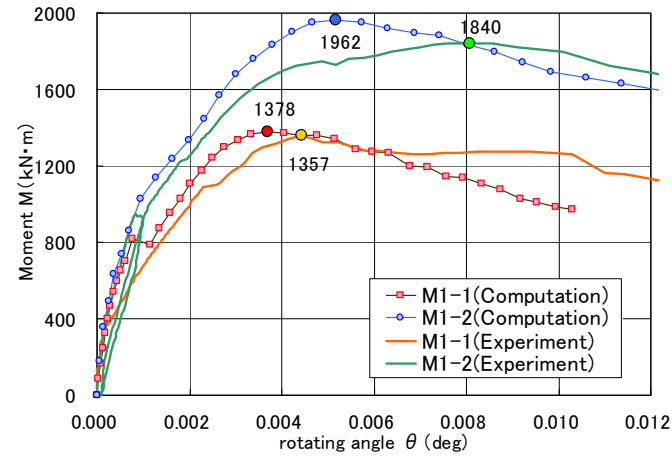


Figure 14. Moment load/rotational angle relationship.

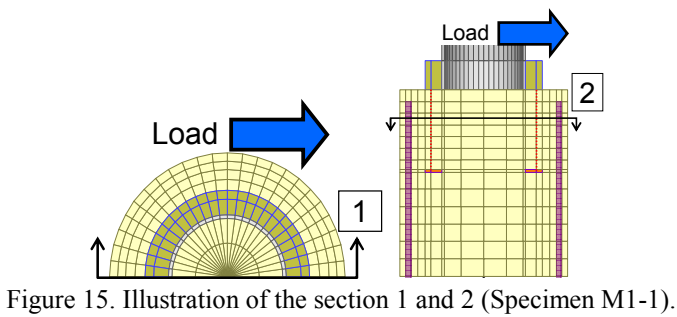
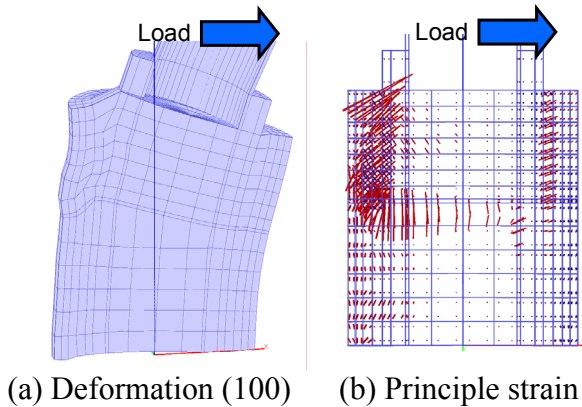


Figure 15. Illustration of the section 1 and 2 (Specimen M1-1).



(c) Cracking in experiment

Figure 16. Computed and experimental results of the section 1 (Specimen M1-1).

All the experimentally observed cracks, i.e. the horizontal cracks that started from the embedded steel plate and splitting cracks and shear cracks both of which started from the steel bolts, can be accu-

ately replicated in the analysis. Figures 16b and 17b show the 1st principal strain vector of each gauss point at the peak load in sections 1 and 2, both of which can be well verified by the crack pattern in the specimen at failure (Figs. 16c~17c).

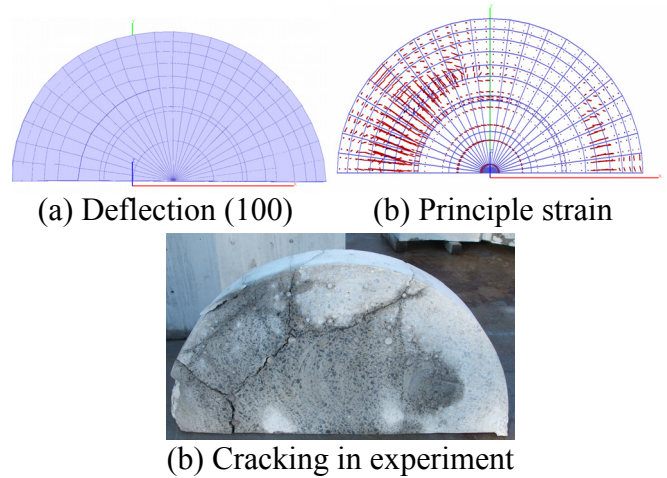


Figure 17. Computed and experimental results of the section 2 (Specimen M1-1).

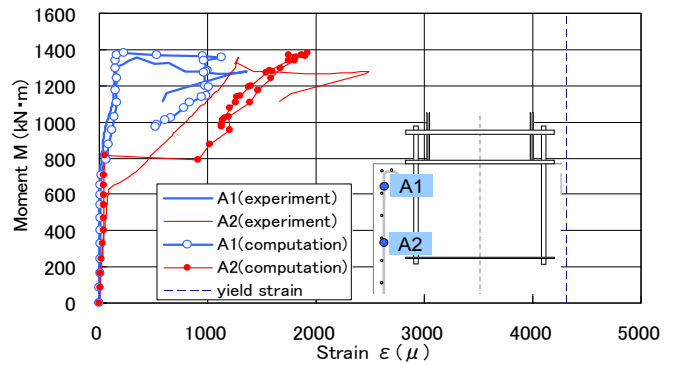


Figure 18. Strain on axial reinforcements (Specimen M1-1).

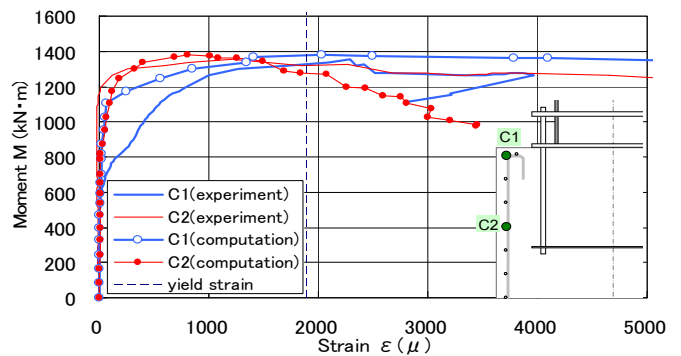


Figure 19. Strain on web reinforcements (Specimen M1-1).

Moreover, the axial and web reinforcement strain can also be accurately simulated in the analysis as shown in Figures 18 and 19. No axial reinforcement yielded in the analysis while all web reinforcement on the tension side of the concrete specimen yielded in the analysis. It can be readily understood that – similar to the general bond behavior of deformed bars – the pull out capacity would come when the web reinforcement yields in the concrete cover.

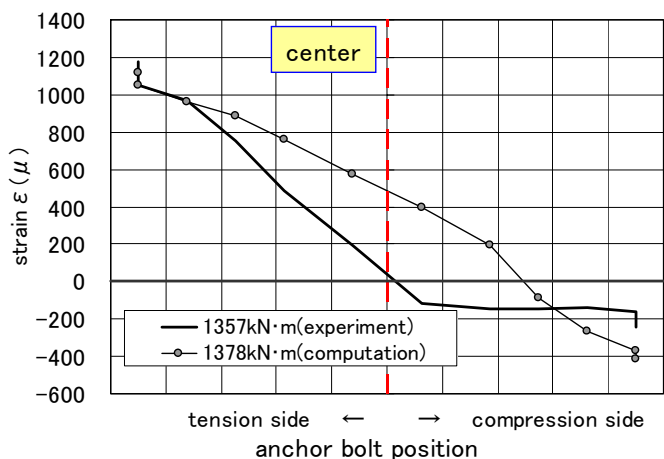


Figure 20. Distribution of Anchor bolt strain (Specimen M1-1).

Distribution of Anchor bolt strain when the moment load is about at its maximum is also well simulated in the analysis as shown in Figure 20. The distribution shape of the anchor bolt strain is almost triangular. It implies that the peak moment of the specimen is dominated by the pull out capacity of the anchor bolt at extreme tension side.

Based on all the simulated results above, the analysis reveals that splitting cracks reduce the pull out capacity of anchor bolt at tension side and bring on the failure of whole anchorage system.

4 DISCUSSION

Based on experimental results, Yoshii et al. (1998) proposed an equation to predict the pull-out capacity of a steel leg on a conventional transmission tower embedded in a caisson-type foundation. As shown in Figures 21 and 22, as the conventional tower leg tends to be pulled out, the rib of the leg will produce horizontal cracks and splitting cracks in the concrete cover and such anchorage system will fail when the internal shear crack penetrates the concrete cover.

The maximum uplift load of a single steel leg with rib can be calculated by Yoshii et al. (1998) as follows:

$$P = \frac{2 \cdot \pi \cdot \alpha \cdot \beta \cdot \gamma \{ (D - \phi) / 2 \} \cdot L_e \cdot f_t}{\tan \theta} \quad (3)$$

where P is the anchoring capacity, D is the concrete body diameter, ϕ is the diameter of the tower leg, L_e is the effective development length, f_c is the compressive strength of concrete, f_t is the tensile strength of concrete, and θ is the angle of the reaction force.

Here, α , β and γ are parameters that take into account the effects of the size of the concrete cover, concrete strength, and effective development length respectively. The formulae are listed as follows:

$$\alpha = 1.5 \{ (D - \phi) / 2 \}^{-1/3} \quad (4)$$

$$\beta = 6.3 \cdot f_c^{-1/3} \quad (5)$$

$$\gamma = 1.2 \{ L_e / \phi \}^{-1/7} \quad (6)$$

It can be noted that the failure mechanism of the single-pole tower foundation is similar to the conventional caisson-type foundation. Hence, Equations (3)~(6) can be adopted to evaluate the pull-out capacity of the anchor bolt system for single-pole towers. Here, the whole system with the anchor plate is equivalent to the steel pipe in Figure 21. Therefore, it can be formulated as follows:

$$P = \frac{2 \cdot \pi \cdot \alpha \cdot \beta \cdot \gamma \{ (D - \phi) / 2 \cdot L \cdot f_t \}}{\tan \theta} \quad (7)$$

$$\phi = D_2 \quad (8)$$

where D_2 denotes the distance between the anchor bolt embedded in the two opposite sides of the concrete body.

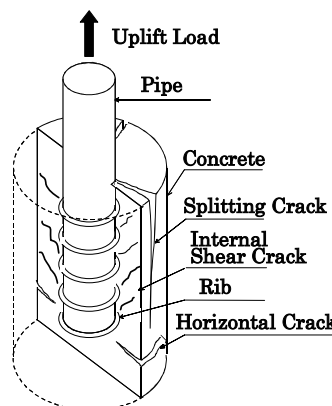


Figure 21. Failure mode of concrete body due to uplift load.

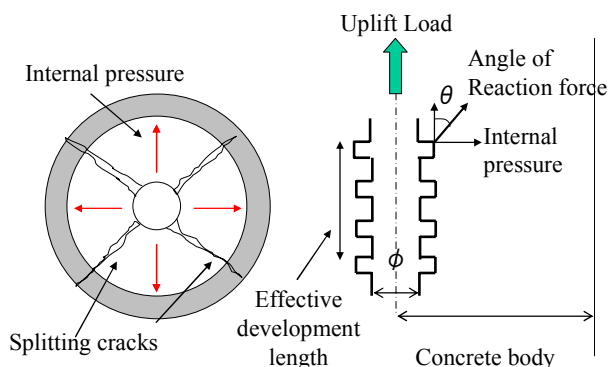


Figure 22. Model of splitting due to uplift load.

Differently from the above, a moment load has to be applied to the single-pole tower foundation. The strain distribution on different anchor bolts around the circumference is shown in Figure 20 and 23,

which can be seen that the strain distribution appears a triangular shape at its limit.

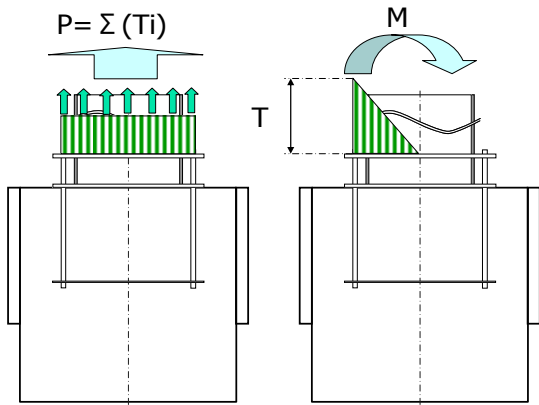


Figure 23. Transfer model of splitting due to moment load.

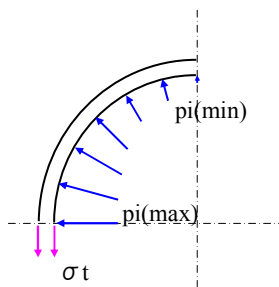


Figure 24. Inner pressure due to moment load.

Table 4. Comparison of between-experimental and proposed equation values.

No.	Maximum moment (kN•m)		Ratio P_{ex}/P_p
	Experiment P_{ex}	Proposed value P_p	
M1-1	1,357	1,230	1.10
M1-2	1,840	1,491	1.23

Based on the triangular shape assumption and actual position of each anchor bolt in the experiment, the total tensile force of anchor bolts can be calculated:

$$\sum T_i = 0.66 \sum T_{max} \quad (9)$$

Here, T_i means the tensile force of each anchor bolt in the bending case, and T_{max} means the tensile force of each anchor in the pure tension case.

Besides, triangular shape of inner pressure would be produced along the circumference in the bending case (Figure 24). The tensile stress induced in the concrete cover can be calculated:

$$\sigma_{tb} = 0.52 \sigma_{tmax} \quad (10)$$

Thus, the average tensile force T' of each anchor bolt is computed as follows:

$$T' = T \cdot (0.66 \cdot 0.52) = 0.34 \cdot T$$

Therefore

$$T \approx 3 \cdot T' = 3P/n \quad (11)$$

where n denotes the number of anchor bolts.

Therefore, the maximum moment that can be applied to the foundation can be calculated as:

$$M = \frac{I}{y} T = \frac{I}{y} \frac{3P}{n} = \frac{3I}{yn} \left(\frac{2 \cdot \pi \cdot \alpha \cdot \beta \cdot \gamma \{ (D-\phi)/2 \cdot L \cdot f_t \}}{\tan \theta} \right) \quad (12)$$

where M is the moment load, I is the moment of inertia of a cross-sectional area of the anchor bolt group, and y is the distance from the neutral axis.

Table 4 shows the experiment capacity and the computed value of the proposed equation. Although some gap still exists between the experiment results and computed values, it can still be used for the primary design stage.

5 CONCLUSION

Both experimental and analytical studies are performed to understand the failure mechanism of single-pole tower foundations. Unlike conventional types of foundation with embedded steel legs, the anchorage system for a single-pole tower is subject to moment loads; thus, only the anchor bolts embedded in the tension side of the concrete body tend to be pulled out. Similar to the conventional type of foundation, both horizontal and splitting cracks can be found in the concrete cover. After yielding of the web reinforcements, which govern the splitting crack width, the anchorage system will soon reach its capacity and fail when internal shear cracks propagate to the surface. It is also found that the confinement level significantly affects the anchorage capacity. M1-2 with its wider reinforced concrete cover could bear a much larger moment load than M1-1. Thus, enlarging the concrete cover with reinforcements would be a practical strengthening method considering the narrow space available for construction.

3D FEM analyses by COM3, which incorporated the full path-dependent modeling of nonlinearity of reinforced concrete, can successfully simulate the experiment results and be used as a design tool for single-pole tower foundations. Both capacity and failure modes of both cases could be successfully captured by numerical analyses as well as the cracking pattern and steel strain, which implied that the dilatant effect inside the concrete core was the source of splitting crack.

Based on the similarity of the failure mechanism, the design formula used for conventional tower foundations is extended to the single-pole type. Also, as the computed maximum moment roughly matches the experiment results, this implies that it can be

used in the primary design of single-pole tower foundations.

REFERENCES

- Okamura, H. and Maekawa, K. 1991. *Nonlinear Analysis and Constitutive Models of Reinforced Concrete*. Gihoudou-Shuppan, Japan.
- Maekawa, K., Pimanmas, A. and Okamura, H. 2003. *Nonlinear Mechanics of Reinforced Concrete*. Spon Press, London.
- Yoshii, Y., Iijima, M., Saito, S. and Matsushima, M., "Experimental study on bond of anchor pipe with ribs embedded in the caisson type foundation," *Journal of Materials, Concrete Structures and Pavements, JSCE*, 606/41, 1998, pp 129~140.
- You, W., Han, T., Wang, H. and Yu, C. 2004. Pre and Post Processor for 3D Nonlinear FEM Analysis of RC Structures. In An, X., Ma, Z., Song, W. and Hirota, F. (eds) *Innovative Application of Information Technology in Construction*. Tsinghua Univ. Press, Beijing.